2008

First observations of turbulence generated by grass fires

Craig B. Clements, *San Jose State University*
Shiyuan Zhong, *Michigan State University*
Xindi Bian, *Northern Research Station, USDA Forest Service*
Warren E. Heilman, *Northern Research Station, USDA Forest Service*
Daewon W. Byun, *University of Houston*

First observations of turbulence generated by grass fires

Craig B. Clements,[1] Shiyuan Zhong,[2] Xindi Bian,[3] Warren E. Heilman,[3] and Daewon W. Byun[4]

Received 22 February 2008; revised 5 July 2008; accepted 23 September 2008; published 20 November 2008.

[1] Wildland fires radically modify the atmospheric boundary layer by inducing strong fire-atmosphere interactions. These interactions lead to intense turbulence production in and around the fire front. Two field experiments were conducted in tall-grass fuels to quantify turbulence generation during the passage of wind-driven fire fronts. Observations showed that the measured turbulence generated by the fires was five times greater than the turbulence in the ambient environment. The production of the turbulence at the surface near the fire front was caused by increased variance of the ambient wind, while the buoyancy was strongest at higher levels within the fire plume. Immediately after the fire front passage, turbulence kinetic energy decreased to ambient levels and was associated with strong downdrafts that occurred behind the fire front.

Citation: Clements, C. B., S. Zhong, X. Bian, W. E. Heilman, and D. W. Byun (2008), First observations of turbulence generated by grass fires, *J. Geophys. Res.*, *113*, D22102, doi:10.1029/2008JD010014.

1. Introduction

[2] Throughout the world wildland fires annually cause significant loss to life and property. While forest fires are more intense, destroy major resources, and tend to gain media attention due to their larger scale, grass fires on the other hand, can spread at amazingly fast rates causing extremely dangerous conditions to fire fighters and to communities located within these environments. In 2006, grass fires caused major loss of life and property in the Great Plains of the United States [*Weaver*, 2006].

[3] Over the past three decades various models have been developed to describe fire behavior as an aid to fire management. Most of these models, however, are empirically derived and emphasize fuels and basic weather conditions reflected only by surface temperature, humidity and wind. While these models have shed some light on fire spread in simple fuels and terrain types, they lack the sophistication needed to fully describe fire-atmosphere interactions.

[4] In recent years significant progress has been made in simulating wildland fires using coupled fire-atmosphere models. These models employ a variety of methods including the coupling of empirical fire-spread models with high-resolution atmospheric models [*Clark et al.*, 1996], the coupling of a higher-resolution combustion model with an atmospheric model [*Morvan and Dupuy*, 2001], and entirely physically based three-dimensional models that account for more physical processes and transport [*Linn et al.*, 2002; *Mell et al.*, 2007]. A more comprehensive review of coupled fire-atmosphere models can be found in the studies of *Linn and Cunningham* [2005] and *Sun et al.* [2006].

[5] While coupled fire-atmosphere models have been shown to successfully simulate fire spread characteristics in simple fuels, simulating the detailed structure of the fire-atmosphere interface, however, has remained a challenge. This is due in part to the lack of observations available at that scale for model validation. Therefore measurements obtained at the fire-atmosphere interface that include fine-scale flows and turbulence would provide a much needed means of validating these models.

[6] Measurements close to wildland fires are difficult to make in any circumstance. This difficulty is based on both safety and logistical issues associated with the complex environment that a fire of any scale manifests. The lack of measurements in and around fires creates a major obstacle in developing realistic fire behavior models. Compared to wildland fires, prescribed burns are usually less intense and offer a more controlled situation. Still, there are inherent difficulties in making measurements in and around fires and studies to date are limited [*Clements et al.*, 2006].

[7] While there have been some large experimental efforts aimed at understanding wildland fire dynamics [*Wilmore et al.*, 1998; *Radke et al.*, 2000; *Coen et al.*, 2004], few studies, however, have focused on the fire-atmosphere interface and even fewer have obtained high-frequency wind and temperature measurements needed to determine the turbulence structure associated with wildland fires. Of these few studies, the International Crown Fire Modeling Experiment, ICFME [*Alexander et al.*, 1998], collected a wide variety data from numerous experimental crown fires. While this campaign did measure in-situ wind, temperature and radiation it did not capture high frequency measurements of the flow needed to estimate the turbulent

[1]Department of Meteorology, San José State University, San José, California, USA.
[2]Department of Geography, Michigan State University, East Lansing, Michigan, USA.
[3]Northern Research Station, USDA Forest Service, East Lansing, Michigan, USA.
[4]Institute of Multidimensional Air Quality Studies, Department of Geosciences, University of Houston, Houston, Texas, USA.

0148-0227/08/2008JD010014

fluxes associated with the experimental fires. However, *Clark et al.* [1999] were able to calculate small-scale velocities and heat fluxes using high-resolution infrared video imagery. This study was most likely the first to estimate vertical velocities associated with a crown fire.

[8] A number of studies have focused on fire growth and spread in grassland environments [*Cheney et al.*, 1993; *Cheney and Gould*, 1995]. These studies were conducted in Australia on a number of plots that ranged in size from 50 to 300 m. These experiments are often used to validate numerical simulations of fire spread in grass fuels [*Sun et al.*, 2006; *Mell et al.*, 2007] and are frequently referred to as the Australian grass fire experiments. While the Australian experiments were well documented in regards to fire behavior and spread, these experiments lacked measurements of the flow and temperature fields within the experimental plots. Furthermore, the meteorological measurements that were made around the plots did not have fast enough sampling rates required to estimate turbulent quantities.

[9] The most comprehensive observational studies that have focused on turbulence and microscale flows and temperature fields within a plume induced by an intense heat source were those by *Bénech* [1976], *Bénech et al.* [1986], *Noilhan and Bénech* [1986], and *Noilhan et al.* [1986]. These studies were conducted to understand the impacts of waste heat releases from cooling towers. The heat source was an array of oil burners which provided 1000 MW of dry heat to the atmosphere. Although these plume studies were conducted using an artificial heat source, the plume properties are most likely similar to that generated by a wildfire except that during an actual wildland fire the heat source is not stationary because of the movement of the fire front. These studies showed that the plume initiated by the heat source was characterized by reduced pressure within the core of $\sim$1 hPa that were well correlated to large vertical velocities. They also showed the importance of the pressure gradient term and that it acts to accelerate the plume near the heat source and reduce the buoyancy in the upper levels. Furthermore, their studies showed strong convergence in the lower portions of the plume and that this mechanism caused the plume to go into rotation. The strong vorticity found within the plume was associated with a reduction of entrainment into the column. These studies provide some guidance on how a plume initiated by a large heat source interacts with the surrounding atmosphere. They do not, however, represent a real fire ignited in natural fuels nor its interaction with the atmosphere.

[10] In this paper, we present first in-situ observations of turbulence characteristics of fire plumes associated with the passage of fast-moving fire fronts during two grass fires. Detailed turbulence measurements were obtained during two separate prescribed experimental fires conducted approximately one year apart on the same site under similar fuel and meteorological conditions. Both prescribed burns were conducted to resemble actual wildland fires in that the fire was allowed to spread with the wind and through the instrumentation. The motivation for these experiments, which are quite difficult to conduct, is to improve our understanding of the structure and characteristics of turbulence at the fire-atmosphere interface. A better understanding of the turbulent nature of fire behavior has the potential for saving lives. Further, the data set can be used to validate dynamic coupled fire-atmosphere models.

[11] This paper is organized as follows. In section 2 we describe the experimental setup including the field site, instrumentation, data processing, fuel and synoptic conditions. Results are presented in section 3, a discussion follows in section 4, and conclusions are drawn in section 5.

2. Experimental Setup

[12] In this section we provide the background information for the two experiments, the 2005 Pilot Study and the 2006 FireFlux experiment, which include the field site, experimental design, instruments and configuration used, fuel characteristics, synoptic weather conditions and data processing procedures.

2.1. Field Site

[13] The experimental burns took place on a 155-acre native tall-grass prairie located at the University of Houston's Coastal Center (HCC) in central Galveston County, Texas approximately 45 km southeast of the Houston metropolitan Area. The experimental prairie is a rectangle that is approximately 970 m long from north to south and is approximately 400 m wide from east to west. Typically, the prairie is managed by mowing every year in the fall and prescribed burning every 2–5 years. For these experiments the prairie was burned on 17 February 2005 (Pilot Study) and again on 23 February 2006 (FireFlux Experiment).

2.2. Experimental Design and Measurement Strategy

[14] During the Pilot Study in 2005 a limited number of instrumentation was available, while the FireFlux experiment was more extensively instrumented in order to fully capture and characterize the turbulent nature of the fire-atmosphere interface. A majority of the discussion on instrumentation will be focused on the FireFlux experiment with reference to the Pilot Study when appropriate.

[15] During both experiments, turbulence measurements were made using a 43-m flux tower located within the burn perimeter. This flux tower, referred to as the main tower, is a permanent, guyed, Rohn-type 45G tower and is located approximately 100 m from the northern edge of the prairie (Figure 1). During FireFlux, a second 10-m portable flux tower was also deployed to approximately 300 m south of the main tower (Figure 1) to help capture the fire front further downwind. The ambient atmospheric vertical structure was monitored by an on-site tethersonde system and a sodar (SOund Detection and Ranging). A number of additional instruments were also used during FireFlux, which included a radiosonde sounding system, a second sodar, a portable weather station, digital still and video photography equipment, and an infrared digital video imagery system. Further details on these instruments used during the Pilot Study and FireFlux are discussed by *Clements et al.* [2006] and *Clements et al.* [2007].

[16] The experiments were designed to simulate a wind-driven grass fire as closely and safely as possible. During FireFlux, the fuel was ignited as a line fire from the northern edge of the prairie (Figure 1). The ignition started from the center of the line and continued toward each side of the prairie using two two-person crews walking in opposite

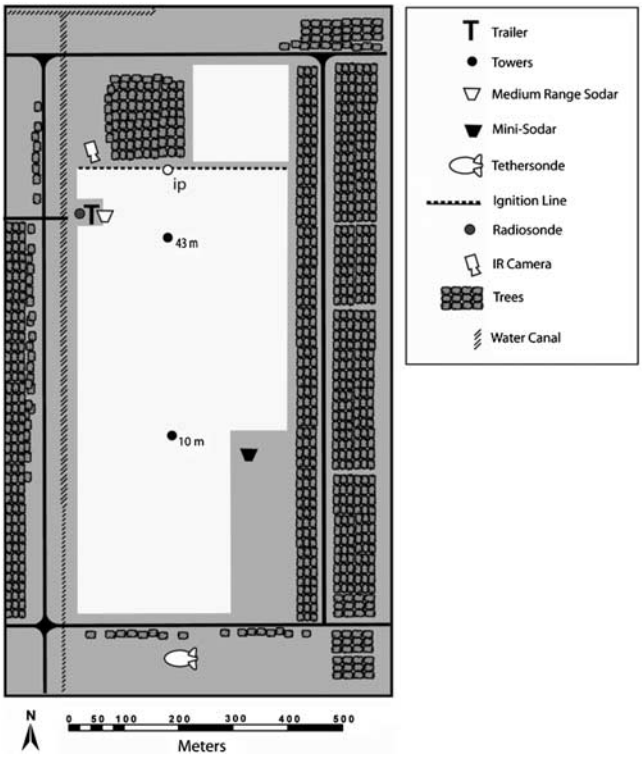

Figure 1. Schematic drawing of experimental layout and instrument locations. The circle labeled ip (ignition point) indicates the location of the start of the ignition line.

directions. The tower arrangement was intended to capture the flow and temperature fields at the fire-atmosphere interface as the fire front traveled with the wind and passed each tower consecutively. Ignition during the Pilot Study began when the burn crew started back burning along the southern (downwind) edge of the burn plot and then continued by creating a black line and back burn around the main tower before the upwind section was ignited. A two-person burn crew on all-terrain vehicles began ignition in the southeast corner of the experimental plot and ignited along the east edge and then continued along the north edge igniting the head fire. The head fire passed the main tower approximately 30 min after the black lining occurred. A more detailed description of the ignition during the Pilot Study is discussed by *Clements et al.* [2006].

[17] Four three-dimensional sonic anemometers (R.M. Young 81000) were mounted on the main tower with one at 2.1 m, 10 m, 28.5 m, and 43 m. At the 10 m and 28.5 m levels, a Li-Cor 7500 open-path gas analyzer was collocated with each sonic to measure both CO_2 and H_2O concentrations. Both the sonic anemometers and the gas analyzers were sampled at 20Hz using Campbell Scientific, Inc. (CSI) CR-5000 data loggers. Fifteen type-T fine-wire thermocouples were mounted on the tower from 0.1 m to 43 m (Omega, Inc. 5SC-TT-40) and sampled using a CSI AM25T multiplexer and averaged to 1 Hz. In addition to the 1 Hz averaged thermocouples, at the 2 m level a very fine-wire type-K thermocouple (Omega, Inc., CHAL-0005) was mounted near the sonic path and was sampled at 20 Hz. Net radiation was measured using a Kipp & Zonen CNR1 four-component net radiometer located at 6.9 m AGL. The soil properties were measured 3 m from the tower base using two soil heat flux plates (REBS, HFT-3) located 8 cm below the ground surface, a soil temperature thermocouple probe (CSI TCAV) located 3 and 10 cm below the surface, and a soil water content probe (CSI CS-616) located 4 cm below the surface. Mean winds, temperature and humidity were measured at four heights on the tower, 2 m, 10 m, 20 m, 43 m using R.M. Young 5103 anemometers and CSI CS-500 temperature/RH probes. These instruments were sampled at 1 Hz using a CSI CR-23X data logger. All data were transferred to one computer located inside the data acquisition trailer over Ethernet via buried fiber optic cable.

[18] The sonic anemometers were mounted on the end of tower cross arms that extended 1.4 m east of the tower. Mean instruments were mounted on cross arms that extended south west from the tower. The R.M. Young 5103 propeller anemometers were mounted 1.4 m from the tower and CS-500 probes were mounted 0.4 m from the tower and housed in a six-plate radiation shield. The line of thermocouples were mounted on the southwest leg of the tower and at each level extended outward approximately 10 cm.

[19] The second tower was a 10-m tower placed 300 m south of the main tower in the middle of the prairie. Two R.M. Young 81000 three-dimensional sonic anemometers were mounted on the tower at heights 2.3 and 10 m AGL. One CSI KH20 hygrometer was colocated with the 2-m sonic. In addition, mean temperature and relative humidity were measured with a Vaisala, Inc. HMP45C probe a 2 m. Soil moisture, soil heat flux and soil temperature were measured using a similar setup as that used at the main tower. Fuel temperatures were measured using three 24 AWG ceramic Type-K thermocouples placed 4 m north of the tower within the fuels at heights of 0.47 m, 0.89 m and 1.4 m AGL. Three 40 AWG Type-T thermocouples (Omega, Inc., 5SC-TT-40) were mounted on the tower at 2, 5, and 10 m AGL. In addition, a very fine-wire thermocouple (Omega, Inc., CHAL-0005) was installed at the sonic path at 2.3 m. All sensors were sampled using a CSI CR5000 data logger at a rate of 20 Hz. The Type K thermocouples were averaged to 1 min and 1 s. The samples from the T/RH were averaged to 1 min. The raw 20 Hz samples from the two sonics, fine-wire thermocouple and KH20 were stored. The 40 AWG thermocouples were averaged to 1 s and the soil sensors were averaged to 1 min. All data were stored on a 2-Gb memory card within the data logger while communications to the logger were made via a CSI RF400 modem. Power was provided by one 12-V deep cycle battery and 128-W solar panel.

[20] Instrumentation used during the Pilot Study was configured differently than the FireFlux experiment. The sonic anemometer (81000) and Li-Cor 7500 were mounted only at 10 m on the main tower and no other turbulence measurements were made. Mean temperature and winds were measured at three locations on the tower, 3, 22, and 32 m. More details of the experimental design from the Pilot Study are discussed by *Clements et al.* [2006].

2.2.1. Preburn Fuel Treatments

[21] The nature of the fire environment required extensive preplanning in the tower configuration and preburn fuel treatment in order to protect equipment from excessive heat and at the same time allow for the measurement of the fire-

atmosphere interface. In addition to instrument protection, data quality was a factor since sonic anemometers fail in high temperature situations. Even with these limitations, sonic anemometers are a very suitable platform to measure the flows and turbulence at the fire-atmosphere interface.

[22] Preburn fuel reduction treatments consisted of either black lining or back burning or by the cutting of fuels from around the instrumentation. Black lining is when the fuels are reduced by burning and thus leaves a black line around the protected area. Back burning consists of a fire that is allowed to burn into the wind and occurs at a much slower rate than a fire burning with the wind. During the Pilot Study both black lining and back burning were used to provide a safety zone 15–20 m around the tower base.

[23] The goal during the FireFlux experiment was to allow the head fire (a fire front driven by the wind) to come as close as possible to the towers, so no active black lining or back burning was used around the towers. Instead, fuels were reduced by cutting around the towers. Fuels were cut down to the surface (0.1 m in height) 5 m out from the base of the main tower and 4 m out from the 10-m tower. Temperature extremes associated with the head fire caused some minor damage and data contamination; however the instrument configuration and fuel treatments performed better than expected. In addition to fuel treatments around the towers, addition protection for the instrument towers, data logger boxes, and cabling was provided by high-temperature ceramic fiber blankets (Cotronics, Inc., 370-2) wrapped around the lower levels of each tower.

2.2.2. Turbulent Calculations and Data Processing

[24] In this study we define turbulence as the perturbation from the mean of any variable. We calculate the turbulence by mean removal from the raw time series data. Thus the turbulence or perturbation from the mean for each velocity component is defined as:

$$u' = u - \overline{u}$$
$$v' = v - \overline{v}$$
$$w' = w - \overline{w}$$

where u is the horizontal velocity in the west-east direction with $+u$ being from the west and $-u$ from the east, v is the horizontal velocity component in the north-south direction with $+v$ being from the south and $-v$ being from the north, and w is the vertical velocity with updrafts being defined by $+w$ and downdrafts by $-w$. The primed variables are the perturbations and the means are denoted by the use of overbars. The mean is subtracted from the time series and we have selected an averaging period of 1 min to isolate the perturbations due to the fire front. Once the perturbations from mean are calculated, we compute the covariance between each of the velocity components to derive the turbulent fluxes. Finally, we Reynold's average the covariances over our selected averaging period.

[25] Post processing of the sonic anemometer data proved to be a challenge since despiking routines would eliminate most of the observed sharp increases in the wind and temperature fields associated with the fire front and plume passage. To overcome this issue, data were bound with maximum and minimum values that were associated with contaminated sonic data. Contaminated data were determined by visual inspection of the raw time series data. After the data were bounded, tilt corrections were applied by use of the planar-fit method [*Wilczak et al.*, 2001], however the u and v components of the wind are not converted to streamwise coordinates but represent the actual east-west and north-south directions. We must add some caution here because of limitations of sonic anemometry. The measurement range of most sonic anemometers is limited by the temperature of the air in which the measurements are made. The maximum measurable temperature of most anemometers is 50°C. Therefore our turbulence data is limited with a minor cold bias due to the instrument's maximum temperature. Surprisingly, the sonic anemometers performed much better than expected, and with the exception of the 10 m level anemometer, very little data was classified as contaminated or above the measurement range of the anemometers.

[26] Wildfires modify their immediate atmospheric environment by emitting large amounts of sensible heat and a combination of gases produced by the combustion of fuels. This will alter the density of the air at the zone of combustion and immediately near the fire front. Following *Coen et al.* [2004] we have neglected the role that temperature and water vapor fluctuations have on density because this fire event is more or less a wind driven event and the entrainment of ambient air into the fire plume reduces the influence of temperature and moisture perturbation on density. This assumption introduces errors in the results. Based on thermocouple measurements on the main tower, the plume temperature ranged between 50 and 200°C. Neglecting pressure perturbation, the corresponding density values would range between 0.7 and 0.9 kg m^{-3}, which would result in an error of 10 to 30%. With the entrainment of ambient air, the actual errors are likely to be smaller.

2.3. Fuel Characterization and Weather Conditions

2.3.1. Fuel Type, Fuel Loading, and Fuel Moisture

[27] The experimental prairie consists of a number of different grass species most of which are native (approximately 90%) including Big Bluestem (*Andropogon gerardi*), Little Bluestem (*Schizachyrium scoparium*), and Long Spike Tridens (*Tridens strictus*). The average height of the fuels was approximately 1.5 m in height. Following *Anderson* [1982] these grass types classify the fuel type as a model 3 fuels type. Total fuel loading (mass of fuel per unit area) was estimated through destructive sampling of ten 0.38 m by 0.38 m plots. Locations of the ten samples were determined via a random walk process near the main tower. Inspection of the entire experimental prairie indicated that the fuels were generally homogenous throughout. The fuel loading for the burn unit was estimated to be 1.08 kg m^{-2} or 4.8 tons per acre.

[28] During the Pilot Study the fuel loading was estimated to be 0.16 kg m^{-2} [*Clements et al.*, 2006]. The prairie was completely mowed during the spring of 2004 and subsequently the fuel loading was lowered. During the day of the burn (17 February 2005) the ground surface was covered by about 10 cm of standing water in many areas of the prairie including that surrounding the main tower. Dead fuel moisture content was estimated to be 8%.

2.3.2. Weather Conditions

[29] To minimize the impact of fire smoke on the local community, the two prescribed burns were conducted under similar weather conditions when the area was under the

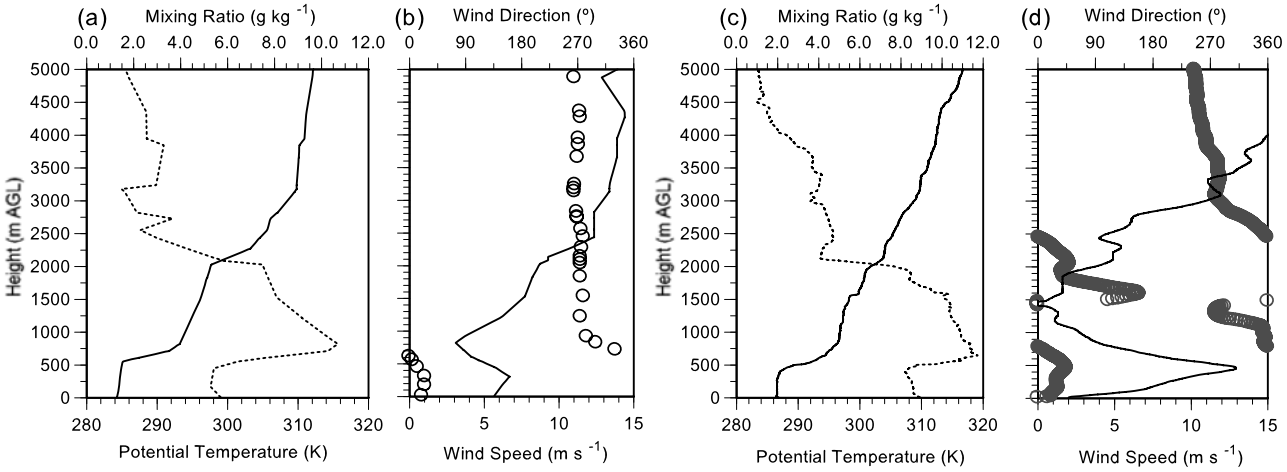

Figure 2. Radiosonde profiles from both experiments. The 2005 Pilot Study (a) potential temperature (solid line), water vapor mixing ratio(dashed line), and (b) wind speed (line) and direction (circles) from Lake Charles, LA 12Z, 17 February 2005. The 2006 FireFlux experiment (a) potential temperature (solid line), water vapor mixing ratio(dashed line), and (b) wind speed (line) and direction (circles) from HCC, 1255Z, 23 February 2006.

control of moderate northeasterly winds. Figure 2 shows radiosonde sounding profiles on the morning of the two experiment days. For FireFlux, which occurred on 23 February 2006, a rawinsonde was released at 0655 LST (1255 UTC) from the experiment site. The Pilot Study took place on 17 February 2005 and occurred when no on-site sounding capability was available; therefore the synoptic conditions were taken from the standard 0600 LST (1200 UTC) sounding at Lake Charles, LA which was the nearest upper-air site. Although nearly a year apart, both days were very similar synoptically. Each experiment occurred in a post cold-front environment with relatively cold and dry air mass and north-northwesterly lower level winds. Vertical potential temperature profiles on both days (Figures 2a and 2c) indicated a neutral layer up to 500 m AGL capped by an inversion of similar strength. The water vapor mixing ratio was larger on the FireFlux day than the day of the Pilot Study; however, both cases exhibited similar vertical structure with a sharp increase of moisture occurring at the level of the capping inversion. Vertical wind structure (Figures 2b and 2d) was also very similar for the two days with a low-level jet 200–300 m AGL from the northeast and westerly winds aloft. Surface winds during both cases were from north-northeast and similar in strength with strong shear in the lowest 500 m AGL.

3. Results and Turbulent Statistics

[30] Results from both the FireFlux experiment and the Pilot Study are presented to show the turbulent structure before, during and after the passage of a fire front and within its induced plume. Data from the two FireFlux towers allow measurements of turbulence during the fire front passage (FFP) at two different locations separated by 300 m in the downwind direction (Figure 1), while the Pilot Study only had one tower location. Photographs of the fire plumes are shown in Figure 3.

Figure 3. Photographs of each experimental fire plume: (a) the Pilot Study back burn around the main tower, (b) the fire front approaching the main tower during the FireFlux experiment, and (c) the dust devil formation during secondary burn of FireFlux (photograph by Laura Hightower).

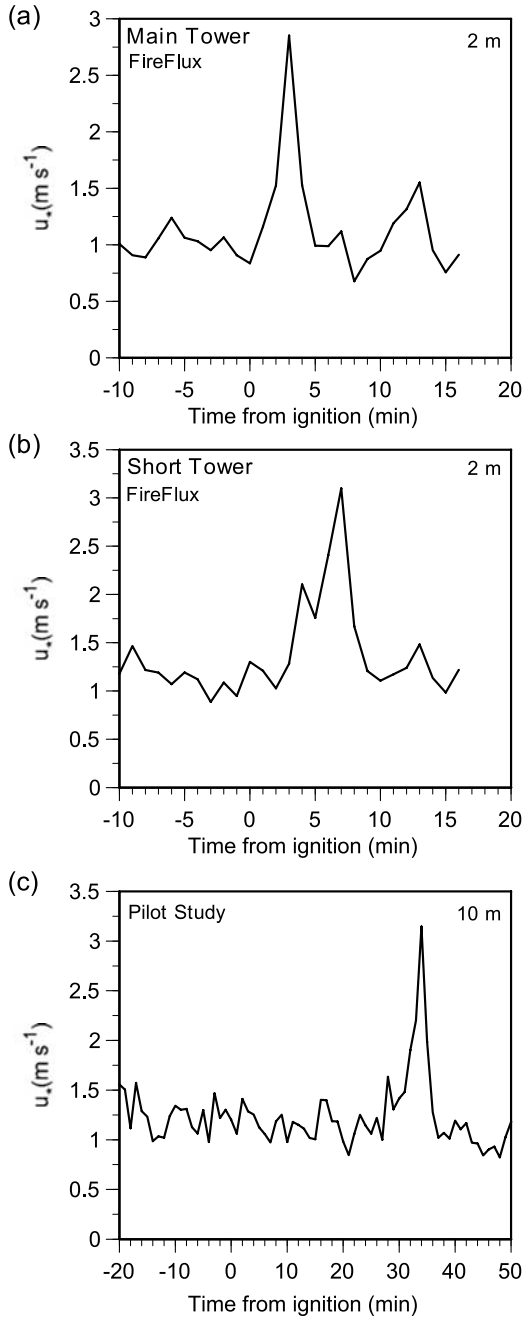

Figure 4. Time series of 2 m u_* values for main tower during FireFlux (a), short tower during FireFlux (b), and 10-m level during the Pilot Study (c).

3.1. Friction Velocity

[31] Friction velocity is the surface stress imposed on the flow when turbulence is generated by wind shear near the ground. The kinematic definition of friction velocity, u_*, is used:

$$u_* = \left[\overline{u'w'}^2 + \overline{v'w'}^2\right]^{1/4} \quad (1)$$

where $\overline{u'w'}$ and $\overline{v'w'}$ are the u and v components of vertical turbulent momentum fluxes. Figure 4 shows the 1-min averaged friction velocity, u_*, plotted relative to the time of ignition for each tower during FireFlux and the Pilot Study. Clearly evident is the dramatic increase in u_* during each fire. This dramatic increase is associated with the FFP. While the background u_* values before the fire are relatively large for near neutral stability, the overall increases associated with the FFP are approximately three times that of the background values for both fires. Values increased from approximately 1–1.5 m s^{-1} to 3–3.5 m s^{-1}. During FireFlux (Figures 4a and 4b) the increases at the main tower occur approximately 3 min after ignition and about 4 min later at the short tower. The increase in u_* during the FFP is followed by a sharp decrease to values similar in magnitude to the observed, ambient, prefire values. A similar increase in u_* is observed later in the fire measured at the short tower located 300 m downwind from the main tower (Figure 4b). The evolution of u_* is similar at both sites indicating that the surface stress is nearly the same for the duration of the fire as it propagates with the wind.

[32] Measurements of u_* during the Pilot Study also show large increase in magnitude that occurred at approximately 35 min after ignition. The ignition time for the Pilot Study includes the initial back burn conducted around the base of the main tower. There is little increase in u_* during the back burn most likely due to the weaker intensity of the fire associated with a back burn (i.e., burning into the wind). When the main head fire plume does reach the tower, the increase in u_* is similar to that of the FireFlux even though the fire passage did not occur as close to the tower as during FireFlux because during the Pilot Study, black lining operations occurred around the tower. Overall the magnitude in u_* during both experiments indicates a strong increase in the turbulent stress associated with the fire front and plume passage. The fire front increases the surface stress on the flow and causes the flow to increase in velocity near the combustion zone leading to increased vertical motion similar to a chimney effect. It is interesting to point out how quickly the u_* returned to its value prior to the fire although there was still smoldering and meandering smoke in the area of the burn. One possible explanation for the quick return of u_* is the response in surface stress due to the fast removal of the surface fuels and change in surface drag. It is worth noting that if the original definition of the friction velocity is used, i.e., $u_* = \sqrt{\left|\frac{\tau}{\rho}\right|}$, the reduction of density as a result of high temperature in fire plume is likely to result in a even larger increase in the friction velocity.

3.2. Turbulence Kinetic Energy

[33] The overall turbulence intensity generated by the fire front and its associated convection plume was determined by analysis of the turbulence kinetic energy or *TKE* obtained from the in situ tower data following [*Stull*, 1988]:

$$TKE = \frac{1}{2}\left(\overline{u'^2} + \overline{v'^2} + \overline{w'^2}\right) \quad (2)$$

where $\overline{u'^2}$, $\overline{v'^2}$, and $\overline{w'^2}$ are the variances of the u, v, and w components of the wind, respectively. Time series plots of 1-min averaged TKE from the measurements of the sonic anemometers on the flux towers during FireFlux and the Pilot Study are shown in Figure 5. In Figure 5a the TKE is

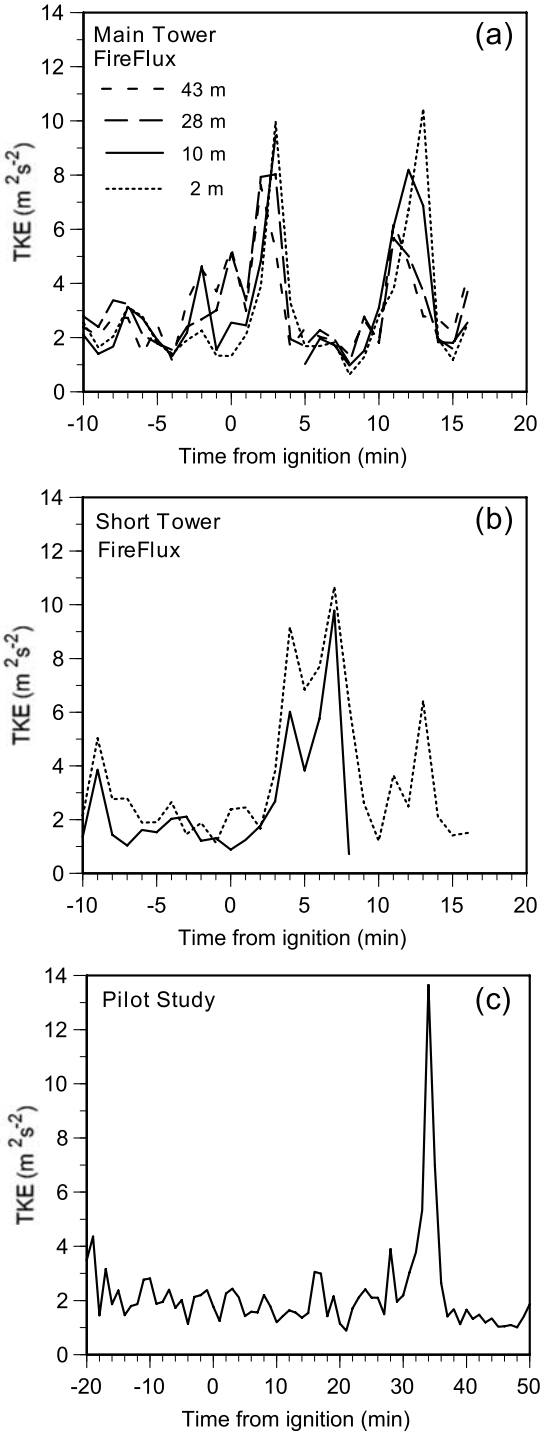

Figure 5. Time series of turbulence kinetic energy for each level on main tower during FireFlux (a), short tower during FireFlux (b), and 10-m level during the Pilot Study (c).

shown for each level on the main tower during FireFlux. Before the fire front passed the tower, there was an initial increase of TKE, mostly in the upper levels of the tower. This initial increase was due to smoke plumes traveling ahead of the main fire front by winds above the prairie. The FFP caused a dramatic increase in TKE values from 2 to 4 m^2 s^{-2} to nearly 10 m^2 s^{-2}, and there is a delay of the TKE jump from upper to lower levels due to the tilted structure of the fire front and associated smoke plumes.

[34] The short tower showed TKE increases occurring 4 min after the fire passed the main tower. There is a dual peak structure (Figure 5b) at the short tower. The first increase was most likely due to turbulence associated with the plume as it was advected downwind of the fire front and the second peak was caused by the actual FFP that occurred 3 min later. The timing of the plume to FFP was similar at both towers. The first increase in TKE at the short tower occurred approximately 1 min after the fire front passed the main tower, suggesting that the downwind distance that the fire-induced plume impacts was at least 200 m in this case. After the FFP, the TKE decreased sharply to near ambient levels. Strong subsidence was found directly behind the fire front, which decreased the turbulence just behind the fire front. This subsidence is most likely a result of mass adjustment due to descending air from aloft that occurred in response to the strong updrafts associated with the fire front. As the air rises above the fire front, air descends to replace it.

[35] The first TKE peak in Figure 5 is a result of a dramatic increase in buoyancy flux due to intense heating associated with the fire front. The second peak in Figure 5, on the other hand, cannot be attributed to buoyancy generation since it happened after the FFP occurred when the heat flux had subsided significantly to only slightly above the prefire level. The fact that the second peak was accompanied by the formation of the dust devil suggests wind shear as the source for the rapid increase in TKE.

[36] The large secondary peak in TKE occurred 15 min after ignition (Figures 5a and 5b). This peak is not associated with the experimental head fire, but rather a burn of a small section of the prairie immediately upwind of the experimental plot that was ignited after the experimental burn was completed. The burn of this small section of the prairie was not part of the original experimental design, but it was done in order to maintain a consistent burn schedule for the entire field. As the plume was moving from northeast toward the south across the field with smoldering from the previous fire present, a dust devil was spotted (Figure 3c) a short distance to the east and southeast of the main tower. A second peak of TKE occurred at the same time when the dust devil appeared. This second TKE peak was seen at both the main and the short tower, although the peak value is smaller at the short tower compared to the main tower.

[37] Evolution of the TKE vertical structure is shown in Figure 6 with averaged periods representing before, during, and after the FFP occurred at the main tower. The vertical profile of TKE before the FFP was nearly constant with height while during the FFP, TKE increased significantly more near the surface than aloft (from approximately 1.5 m^2 s^{-2} to 10 m^2 s^{-2} at 2 m) due to the greater buoyancy generated at the fire front. After the FFP, TKE returned to a near constant profile, but also decreased slightly below the pre-FFP values. The decrease in TKE after the FFP is due to subsidence that was associated with downdrafts occurring behind the fire front. While the downdrafts directly behind the fire front do generate turbulence by inducing strong vertical shearing motions, observers at the flank of the FFP

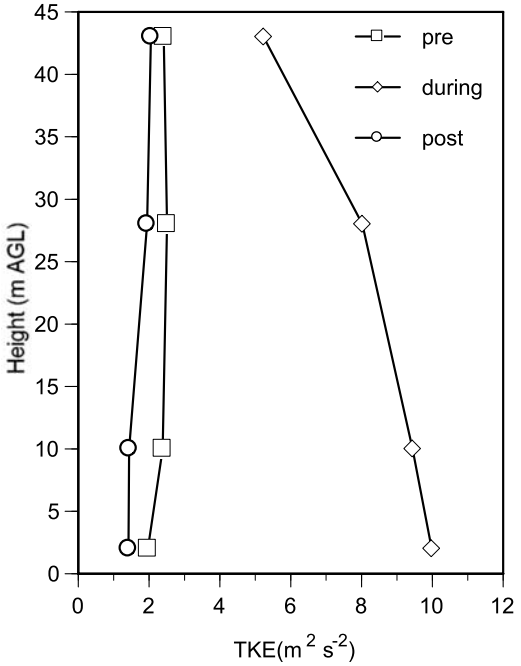

Figure 6. Vertical profiles of TKE for periods before, during, and after the fire front passage.

noted generally weak circulations after the FFP and during the smoldering period afterward.

[38] Figure 7 shows the velocity variances for u, v, and w. During the preignition period of FireFlux (Figures 7a and 7b) both $\overline{u'^2}$ and $\overline{v'^2}$ were larger and fluctuated more than $\overline{w'^2}$, as would be expected for near neutral conditions. As the fire front passed through the main tower, all three velocity variances show a substantial increase in magnitude, with the largest increase associated with $\overline{w'^2}$, indicating that the production of TKE is dominated by convective motion due to strong heating at the fire front. A very large secondary peak in $\overline{v'^2}$ together with a smaller peak in $\overline{u'^2}$ occurred about 13 min after the ignition of the head fire, which correspond exactly to the second peak of TKE shown in Figure 5 and the time when the dust devil was spotted. Little increase in $\overline{w'^2}$ was observed at this time. These observations suggest that the second TKE peak was a result of horizontal wind shear, especially shears in the mean wind direction, as a result of horizontal axis eddies and vortices that developed over the burned field. Fires create strong horizontal pressure gradients that produce convergence and divergence in areas surrounding the fire and the influence on wind speed and direction decreases with the distance away from the fire. These pressure perturbations can produce strong horizontal wind shears that are capable of generating intense turbulence that is as strong as turbulence generated during the passage of a fire front and its associated convection and buoyancy. This may explain why intense turbulence may still exist in the near surface atmosphere after a major fire. This knowledge may help fire fighters or crews in their fire suppression operations.

3.3. Buoyancy Induced by Grass Fires

[39] To better understand the role of buoyancy in the development of turbulence within the fire plume and near the fire-atmosphere interface, we examine the buoyancy flux which is defined as the ratio of sensible heat flux to virtual temperature [*Stull*, 1988]:

$$B_f = \frac{g}{\overline{T_v}}\overline{\left(w'T_v'\right)} \tag{3}$$

where g is gravity, $\overline{T_v}$ is virtual temperature, and $\overline{w'T_v'}$ is the turbulent sensible heat flux. This buoyancy flux is similar to that used by *Sun* [2006] in his idealized numerical simulations of grass fires. However, we do not consider plume radius as *Sun* did. Buoyancy flux was compared for different heights within the plume using the four levels on the main tower during FireFlux and for the 10 m level during the Pilot Study (Figure 8). As the plume impinged on the tower, the buoyancy flux increased dramatically from less than 0.01 to more than 0.8 m^2 s^{-3}. Clearly, the extremely large positive buoyancy flux leads to an intense production of TKE as shown in Figure 5. The buoyancy is greater at higher altitudes of the plume than near the surface. The buoyancy flux at 43 m AGL is 0.8 m^2 s^{-3} which is approximately twice as much as the buoyancy measured at 10 m AGL and even larger than at 2 m near the surface which is due to the tilted plume coming in contact with the tower instruments at higher levels first. All the buoyancy generated from the fire was positive as expected from a fire induced plume. At time of ignition during the Pilot Study the calculated buoyancy flux shows a sharp increase at 1 min after ignition (Figure 8) and then continues to be positive during the period the back burn occurred around the tower. However, the initial increase in buoyancy is not indicated in $\overline{w'^2}$ (Figure 7f). Approximately 30 min later a large increase in buoyancy (0.25 m^2 s^{-3}) occurred during the FFP at the tower.

[40] The observed turbulence kinetic energy during the grass fires increased due to both the variance of the horizontal wind components and the generation of buoyancy. Turbulence within the fire plume, however, is isotropic in nature and equally driven by both buoyancy and wind shear. *Clark et al.* [1996] suggested that buoyancy builds up above and downwind of the fire front. Our measurements show that buoyancy is generated at the combustion zone and transported downwind with the ambient wind. While there is buoyancy production at the fire front as would be expected (Figure 8), shear is also a significant source of TKE. Additionally, the buoyancy flux dropped immediately after the fire front has passed, and thus suggesting that the role of buoyancy in generating turbulence at the fire front is limited to the small region just above the combustion zone.

3.4. Turbulent Momentum Flux and Spectra in Grass Fire Plumes

[41] Turbulence generated by the fire modifies the flow and stress immediately at the fire front and a distance downwind. To determine the role of the fire front on the development of stress on the wind field within and near the fire plumes, 1-min averaged turbulent momentum fluxes were analyzed (Figure 9). Ahead of the fire front $\overline{u'w'}$ was approximately zero near the surface, but as the fire front approached the tower $\overline{u'w'}$ became negative. This negative momentum flux is due to downward transport of higher momentum aloft and this occurred ahead of the fire front

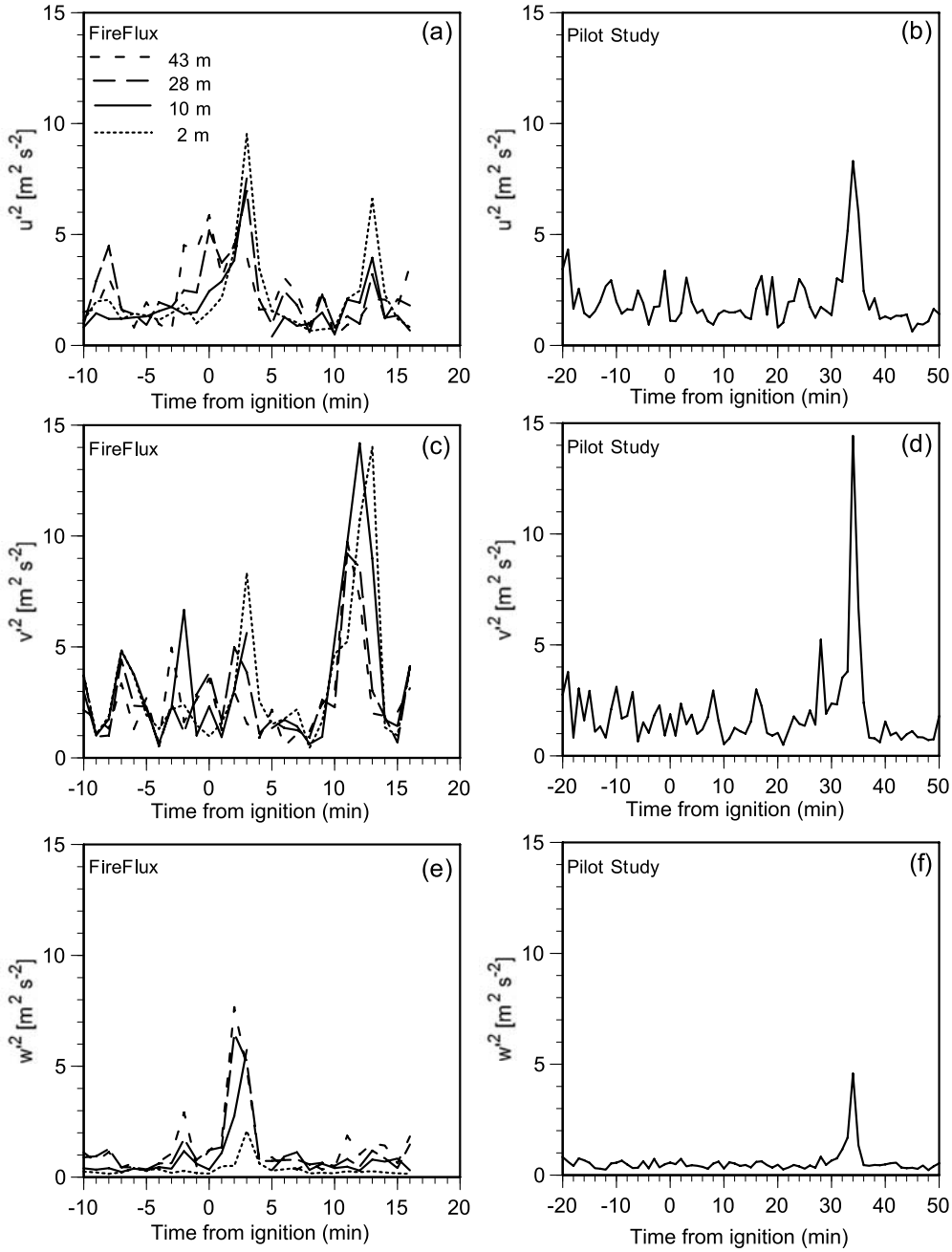

Figure 7. Time series of velocity variances from main tower during FireFlux (a) u, (c) v, and (e) w, and during the Pilot Study (b) u, (d) v, and (f) w.

due to the downdrafts occurring downstream in the tilted plume. Additionally, the recirculation underneath the plume can cause the observed negative momentum flux. Wind shear was quite strong as shown in Figure 2d and supports this observation. However, at higher levels in the plume (28 and 43 m AGL) $\overline{v'w'}$ became positive with a maximum value of approximately 2 m^2 s^{-2} indicating the buoyancy driven updrafts transported stronger momentum from near the surface upward. Additionally, $\overline{u'w'}$ became positive about the same time indicating that the momentum in the upper plume is strongly influenced by positive buoyancy. After about 15 min there is a strong negative covariance in $\overline{v'w'}$ which corresponds to the dust devil passage. Strong horizontal wind variance was shown to also occur during this period (Figure 7c).

[42] During the Pilot Study the momentum fluxes displayed a much more clear response to the FFP by the sharp increase in $\overline{u'w'}$ and with an even more drastic decrease in $\overline{v'w'}$ just as the plume passed the tower. The weak response of the momentum flux at the surface indicates that horizontal momentum was dominated mostly by the ambient wind, while at higher levels within the plume higher momentum was transported from near the surface upward due to buoyancy production. On average, values of $\overline{u'w'}$ are negative, (~ -0.5 m^2 s^{-2}) ahead of the fire front indicating downward momentum transport occurring downstream of

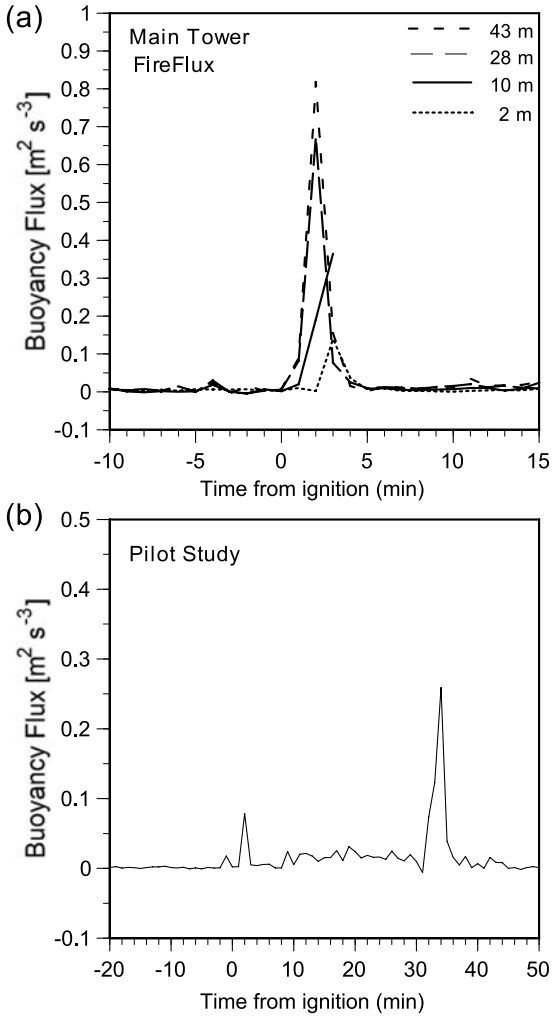

Figure 8. Time series of buoyancy flux during FireFlux (a) and the Pilot Study (b).

the head fire. This corresponds well with photogrammatic analyses of the plume characteristics which also showed strong downward motion well ahead of the fire front.

[43] To determine what role the fire had on the energy spectrum of the vertical momentum, the spectral density log $fS(f)$ is plotted verses the log of the frequency, f, for the w velocity component before, during, and after the fire for the Pilot Study (Figure 10). Although the overall shape of the spectral density did not change, there is a general increase in the spectral density, especially at lower frequencies, indicating the increased contribution to the overall turbulence generation is accomplished by large eddies induced by the fire.

4. Discussion

[44] The observations presented in this paper represent the first published measurements of turbulence generated by natural grass fires. The major purpose of conducting these experiments was to provide a data set for comparing numerical simulations of grass fire dynamics using coupled fire-atmosphere models. While to date there have been few numerical studies that have discussed the modeled turbulence during a FFP, we attempt in this section to relate our observations to the simulations by *Cunningham and Linn* [2007]. The simulations from their study were conducted using the HIGRAD/FIRETEC [*Linn et al.*, 2002] model with a horizontal domain of 320 $\times$ 320 m and a vertical domain of 615 m. Horizontal grid spacing was set at 2 m and the vertical resolution was 1.5 m at the surface increasing to 30 m at the top of the domain. Further details on the model setup can be found in the studies of *Linn and Cunningham* [2005] and *Cunningham and Linn* [2007].

[45] We compare our observed surface velocity wind fields at 1 Hz (Figure 11) with those presented in Figure 6a of the study of *Cunningham and Linn* [2007] (referred to as CL6a and CL07, respectively). CL6a represents the FireFlux experiment most closely with a 3 m s^{-1} ambient wind, a long ignition line, and 1 s model output. In CL07 their u velocity component increased from approximately 0.5 m s^{-1} to over 4 m s^{-1} as the FFP occurred (CL6a). Just before the sharp jump in velocity there was a significant inflow indicated by negative values of u with a magnitude of about 3–4 m s^{-1}. The indraft in CL6a is much greater in magnitude and duration than that observed during FireFlux. The indraft ahead of the fire front during FireFlux occurred only for a few seconds and was extremely weak with a velocity of about 1.5 m s^{-1} at both the Main Tower and the Short Tower (Figures 11c and 11d). The duration of the indraft occurred for about 12 s in CL6a and only 4 s during FireFlux. This difference is due to the fact that surface winds before the FFP observed during FireFlux were about twice that of CL07.

[46] One similarity between CL07 and the observations is the delayed decrease in the u component of velocity after the FFP. This suggests that the entrainment of higher momentum from aloft to the surface occurs even after the fire front passes. During FireFlux the u velocity remains high before decreasing to prefire magnitude, while in CL6a the decrease in u occurs much faster after the passage of the fire front.

[47] The vertical motion simulated by CL07 is very similar to that observed during FireFlux. Comparing Figures 11e and 11f to CL6a, the maximum in vertical velocity during the simulation and in the observation occurred during the FFP as indicated by the maximum in solid fuel temperatures. The magnitude of the positive w component was 6 m s^{-1} in CL6a and between 3 and 4 m s^{-1} during FireFlux (Figure 11f). The simulated velocity was greater than observed and this may be due to the configuration of the reduced fuels around the towers. In CL6a the velocity maximum occurred at the fire front, while during FireFlux, the maximum occurred as the fire front approached and moved around the towers due to the cut fuels region around each tower base. However, it is surprising that the velocity fields are greater in CL6a since the point of model output is taken at z = 0.7 m AGL while our observations are taken at 2.1 m AGL.

[48] Another similarity between CL07 and FireFlux is the occurrence of downdrafts immediately behind the fire front as indicated by the negative w occurring at 170 s in CL6a

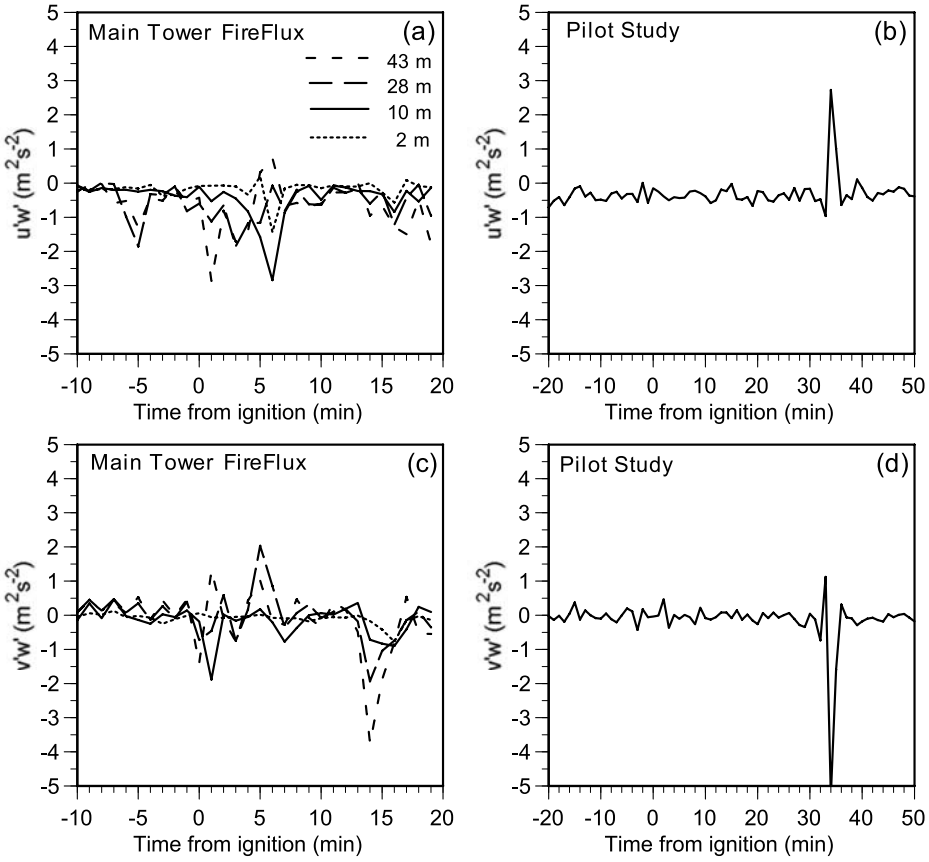

Figure 9. Time series of momentum fluxes during FireFlux (a and c), and the Pilot Study (b and d).

and 8 min in Figure 11f. The magnitude of the downdrafts between FireFlux and CL07 is similar with velocities ranging from 1–2 m s^{-1} and 1–2.5 m s^{-1}, respectively. While downdrafts behind the fireline have also been shown to exist in simulations of grass fires performed by *Sun et al.* [2006], the comparison here illustrates the value of in situ observations for verifying numerical studies.

[49] In addition to the downdrafts that occur behind the fire front, downdrafts were also observed just seconds ahead of the fire front (Figure 11e). This downward motion was associated with the presence of a vortex that formed just ahead of the fire front. The vortex during FireFlux was captured on digital still and video cameras. Simulations from CL07 indicate that the fuels ahead of the fire front are preheated because of the hot gases being recirculated back into the fire front due to the indrafts that form ahead of the fire front. This is most likely a similar circulation as observed in FireFlux.

[50] Finally, we should mention the results of *Bénech et al.* [1986] who found that turbulent fluxes in their experimental burns were 10 times less than the vertical advective flux. They concluded that turbulence was still not yet fully developed at the vicinity of the heat source. Results presented here indicate the opposite. The turbulence is well developed not only in the vertical, but also in the ambient wind which drives the fire spread. This difference may be due to the fact that the plumes analyzed in the *Bénech et al.*

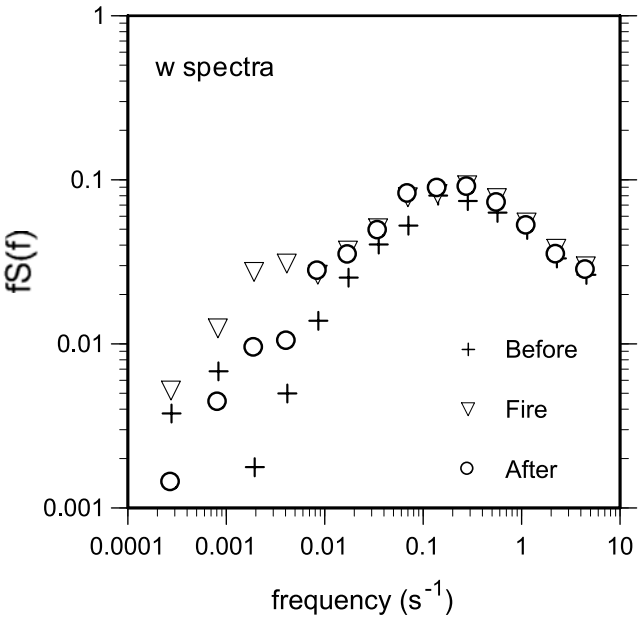

Figure 10. Frequency spectra (m^2 s^{-2}) for *w* component during the Pilot Study and before, during, and after fire.

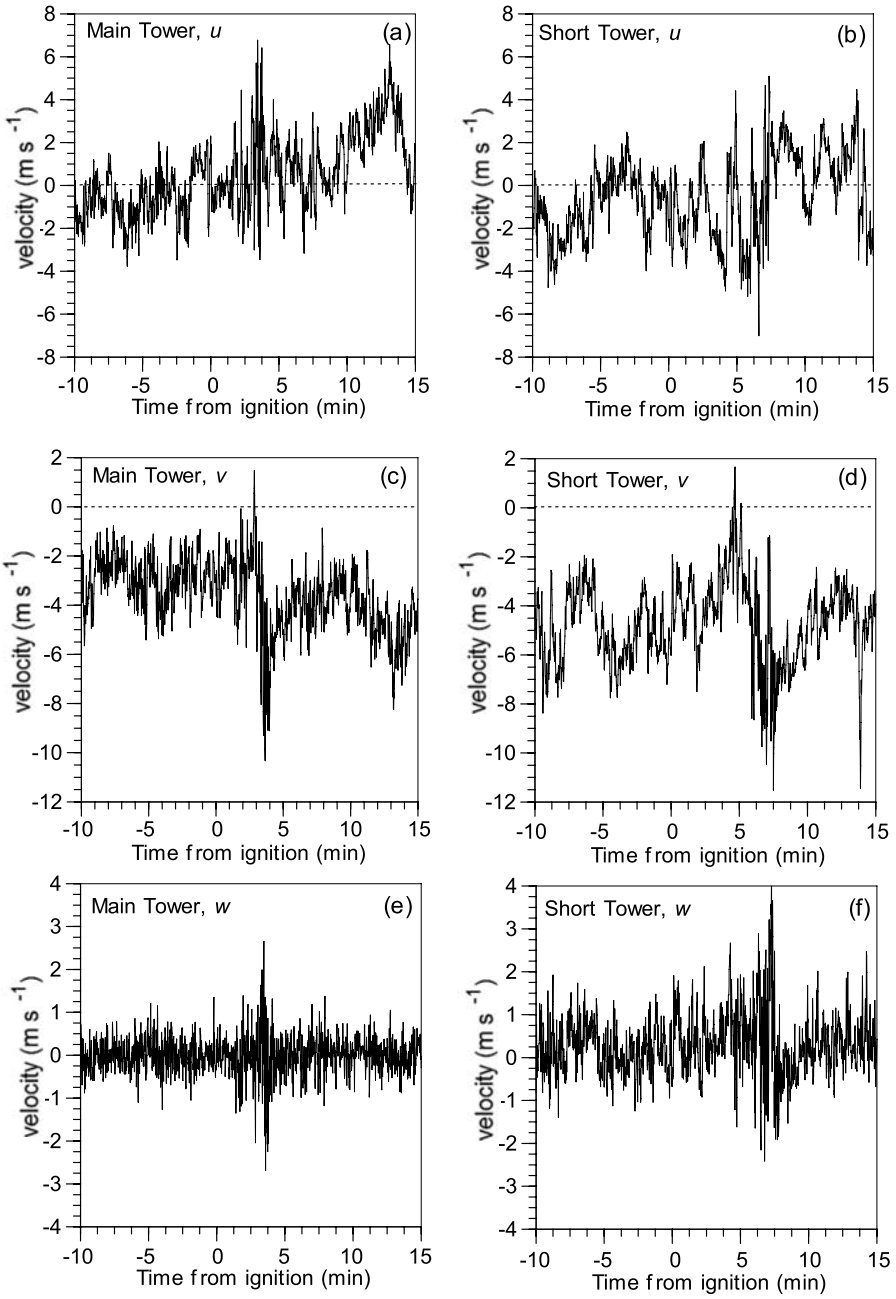

Figure 11. Time series of 1-s averaged 2-m level u (a and b), v (c and d), and w (e and f) wind velocity components at both towers during FireFlux.

[1986] experiments were produced by fixed gas burners and are not really comparable to a heat source that propagates along the surface of the earth such as a natural, wind-driven grass fire.

5. Conclusions

[51] In this paper, first observations of the turbulence generated during grass fires are presented. The analysis of the turbulent statistics was based on in situ measurements made during two grass fires that were conducted on the same experimental prairie consisting of tall-grass fuels. Background meteorological conditions during both experiments were very similar and were associated with post-frontal conditions with near neutral stability.

[52] Observations showed that the measured turbulence intensity generated by the fires was four to five times greater than turbulence in the ambient environment with turbulence kinetic energy increasing from approximately 2 m^2 s^{-2} before the fires to approximately 10 m^2 s^{-2} during the FFP. Additionally, the turbulence kinetic energy that was measured during the formation of a dust devil well after the FFP also suggests that the increased variance in the ambient wind is responsible for the large increase in the generation of turbulence. These observations indicate that wind shear, which is enhanced by a fire-induced increase in velocity of

the surface winds, is capable of generating intense turbulence that is as strong as turbulence generated by the convection of the fire front. After the FFP the turbulence kinetic energy decreased sharply to just below ambient, prefire levels. This decrease in turbulence is associated with subsidence which suppressed the turbulence just behind the fire line.

[53] The behavior of the surface stress, as measured by the friction velocity, u_*, was similar in magnitude and duration at both measurement towers. The overall increase in u_* at the actual FFP was found to be approximately three times that of the ambient values. The turbulence generated at the fire front influenced the downstream turbulence field by the downward transport of higher momentum which occurred just before the arrival of the fire front. This downstream influence was due to the tilted structure of the fire plume and the overall ambient wind shear. The turbulence within the grass fire plumes was associated with a general increase in the spectral density of the w component at lower frequencies suggesting that the contribution by large eddies induced by the fire increased the overall turbulence generation.

[54] The behavior and evolution of surface winds at the fire front observed during these experiments were found to have very similar structure to the grass fires simulated by *Cunningham and Linn* [2007]. However, we do emphasize caution when comparing our observations to numerical models since our observations represent only single points in the fire front and that fuels were reduced around the towers. Future work will continue comparisons with other numerical model simulations. In addition, future observational campaigns set in different fuel types are planned. Comparisons of these future data sets to simulations will be conducted to better understand the mechanisms responsible for the generation of turbulence in wildland fires. With these new observational results, we hope to provide safer fire suppression operations and strategies that can be incorporated in future fire safety protocols.

[55] **Acknowledgments.** We thank Mark Kramer and George Regmond from the Armond Bayou Nature Center for conducting the two experimental burns, Tim Becker from the Houston Coastal Center for helping with the experimental setup and fuel treatments around the prairie, the many students and staff that helped execute both the Pilot Study and the FireFlux field experiments, Dr. Glenn Aumann for his support and use of the Houston Coastal Center for this research, Dr. Scott Goodrick from the USDA Southern Research Station and Dr. Brian Potter from the USDA Pacific Northwest Wildland Fire Sciences Laboratory for their support of this research, Ms. Laura Hightower for her photography support, Mr. Ju Li from the Beijing Institute for Urban Meteorology for the initial data postprocessing while visiting the University of Houston, and the three anonymous reviewers of this paper for their excellent comments and suggestions regarding this research. This work is partially supported by a research grant from the Houston Coastal Center and EPA grant R-82906801. Use of trade names does not imply endorsement by the USDA Forest Service.

References

Alexander, M. E., et al. (1998), The international crown fire modeling experiment: An overview and progress report, preprints, in *Second Symposium on Fire and Forest Meteorology*, pp. 20–23, 11–16 January, Am. Meteorol. Soc., Phoenix, Ariz.

Anderson, H. E. (1982), Aids to determining fuel models for estimating fire behavior, *General Technical Report INT-122*, 22 pp., U.S. Department of Agriculture, Forest Service, Intermountain Forest and Range Experiment Station, Ogden, UT.

Bénech, B. (1976), Experimental study of an artificial convective plume initiated from the ground, *J. Appl. Meteorol.*, *15*, 127–137.

Bénech, B., J. Noilhan, A. Druilhet, J. M. Brustet, and C. Charpentier (1986), Experimental study of an artificial thermal plume in the boundary layer: part I. Flow characteristics near the heat source, *J. Clim. Appl. Meteorol.*, *25*, 418–438.

Cheney, N. P., and J. S. Gould (1995), Fire growth in grassland fuels, *J. Wildland Fire*, *5*, 237–347.

Cheney, N. P., J. S. Gould, and W. R. Catchpole (1993), The influence of fuel, weather and fire shape variables on fire-spread in grasslands, *Int. J. Wildland Fire*, *3*(1), 31–44.

Clark, T. L., M. A. Jenkins, J. Coen, and D. Packham (1996), A coupled atmospheric-fire model: Convective feedback on fire line dynamics, *J. Appl. Meteorol.*, *35*, 875–901.

Clark, T. L., L. Radke, J. Coen, and D. Middleton (1999), Analysis of small-scale convective dynamics in a crown fire using infrared video camera imagery, *J. Appl. Meteorol.*, *38*, 1401–1420.

Clements, C. B., B. E. Potter, and S. Zhong (2006), In-situ measurements of water vapor, heat, and CO_2 fluxes within a prescribed grass fire, *Int. J. Wildland Fire*, *15*(3), 299–306.

Clements, C. B., et al. (2007), Observing the dynamics of wildland grass fires: Fireflux—a field validation experiment, *Bull. Amer. Meteorol. Soc.*, *88*(9), 1369–1382.

Coen, J., S. Mahalingam, and J. Daily (2004), Infrared imagery of crown-fire dynamics during FROSTFIRE, *J. Appl. Meteorol.*, *43*, 1241–1259.

Cunningham, P., and R. R. Linn (2007), Numerical simulations of grass fires using a coupled atmosphere-fire model: Dynamics of fire spread, *J. Geophys. Res.*, *112*, D05108, doi:10.1029/2006JD007638.

Linn, R. R., and P. Cunningham (2005), Numerical simulations of grass fires using a coupled atmosphere-fire model: Basic fire behavior and dependence on wind speed, *J. Geophys. Res.*, *110*, D13107, doi:10.1029/2004JD005597.

Linn, R., J. Reisner, J. J. Colman, and J. Winterkamp (2002), Studying wildfire behavior using firetec, *Int. J. Wildland Fire*, *11*, 233–246.

Mell, W., M. A. Jenkins, J. Gould, and P. Cheney (2007), A physics-based approach to modelling grassland fires, *Int. J. Wildland Fire*, *16*, 1–22.

Morvan, D., and J. L. Dupuy (2001), Modeling of fire spread through a forest fuel bed using a multiphase formulation, *Combust. Flame*, *127*, 1981–1994.

Noilhan, J., and B. Bénech (1986), Experimental study of an artificial thermal plume in the boundary layer: part III. Dynamic structure within the plume, *J. Clim. Appl. Meteorol.*, *25*, 458–467.

Noilhan, J., B. Bénech, G. Letrenne, A. Druilhet, and A. Saab (1986), Experimental study of an artificial thermal plume in the boundary layer: part II. Some aspects of the plume thermodynamical structure, *J. Clim. Appl. Meteorol.*, *25*, 439–457.

Radke, L. R., T. L. Clark, J. L. Coen, C. Alther, R. N. Lockwood, P. J. Riggin, J. Brass, and R. Higgins (2000), The wildfire experiment (WiFE): Observations with airborne remote sensors, *Can. J. Remote Sens.*, *26*, 406–417.

Stull, R. B. (1988), *An Introduction to Boundary Layer Meteorology*, 666 pp., Kluwer Acad., New York.

Sun, R. (2006), Numerical modeling of the effects of fire-induced convection and fire-atmosphere interactions on wildfire spread and fire plume dynamics, Ph.D. thesis, 142 pp., University of Utah, Salt Lake City, Utah.

Sun, R., M. A. Jenkins, S. K. Krueger, W. Mell, and J. J. Charney (2006), An evaluation of fire-plume properties simulated with the FDS and Clark coupled wildfire model, *Can. J. For. Res.*, 2894–2908.

Weaver, T. (2006), A word to the firewise, *Wildland Firefighter*, *10*(7), 25–30.

Wilczak, J. M., S. P. Oncley, and S. A. Stage (2001), Sonic anemometer tilt correction algorithms, *Boundary Layer Meteorol.*, *99*, 127–150.

Wilmore, R., K. Slaughter, M. Theisen, and J. Roessler (1998), FROST-FIRE research prescribed burn plan, 62 pp., Bureau of Land Management Alaska Fire Service.

X. Bian and W. E. Heilman, Northern Research Station, USDA Forest Service, 1407 S. Harison Road, Room 220, East Lansing, MI 48823, USA.

D. W. Byun, Institute of Multidimensional Air Quality Studies, Department of Geosciences, University of Houston, 4800 Calhoun Road, Houston, TX 77204, USA.

C. B. Clements, Department of Meteorology, San José State University, One Washington Square, San José, CA 95192, USA. (clements@met.sjsu.edu)

S. Zhong, Department of Geography, Michigan State University, 208 Geography Building, East Lansing, MI 48824, USA.